

Shannon entropy at avoided crossings in the quantum transition from order to chaosF. J. Arranz,^{1,*} R. M. Benito,^{1,†} and F. Borondo^{2,3,‡}¹*Grupo de Sistemas Complejos, Universidad Politécnica de Madrid, av. Puerta de Hierro 2–4, 28040 Madrid, Spain*²*Instituto de Ciencias Matemáticas (ICMAT), Cantoblanco, 28049 Madrid, Spain*³*Departamento de Química, Universidad Autónoma de Madrid, Cantoblanco, 28049 Madrid, Spain*

(Received 8 April 2019; published 12 June 2019)

Shannon entropy is studied for the series of avoided crossings that characterize the transition from order to chaos in quantum mechanics. In order to be able to study jointly this entropy for discrete and continuous probability, calculations have been performed on a quantized map, the kicked Harper map, resulting in a different behavior, as order-chaos transition takes place, for the discrete (position representation) and continuous (coherent state representation) cases. This different behavior is analyzed in terms of the distribution of zeros of the Husimi function.

DOI: [10.1103/PhysRevE.99.062209](https://doi.org/10.1103/PhysRevE.99.062209)**I. INTRODUCTION**

Since first introduced by Shannon in his *mathematical theory of communication* [1,2], the so-called Shannon entropy, which was defined as a measure of the amount of information (or uncertainty) in the framework of information theory, has been widely used in different fields beyond the theory of information.

In particular, among the applications of Shannon entropy to quantum mechanics, it has been studied for avoided crossings between energy levels, avoided crossings being a central issue in the field of quantum chaos [3]. Shannon entropy at avoided crossings was early studied in the hydrogen atom in the presence of strong magnetic fields [4] and in the presence of strong parallel magnetic and electric fields [5]. More recently, this subject has been studied in the calculation procedure of the multiconfiguration Dirac-Fock method [6], in Rydberg potassium atoms interacting with a static electric field [7], in lattice many-body quantum systems with time evolution [8], and in closed and open quantum billiards [9].

Moreover, it has been shown in the literature that the quantum transition from order to chaos is characterized by certain series of quantum resonances (avoided crossings), related to the corresponding classical resonances (chains of islands), leading to a frontier of scars between order and chaos [10–12], which can be identified through the distribution of zeros of the Husimi function. The Husimi function is the probability density function in the coherent state representation (quantum phase space). Under certain conditions, namely, quantum systems having a two-dimensional compact phase space, it was rigorously proven that, except for the normalization factor, the coherent state representation can be expressed (by means of the Weierstrass-Hadamard factorization of entire functions) in terms of the zeros of the Husimi function [13,14]; that

is, under these conditions, the distribution of zeros of the Husimi function determines the quantum state. Beyond these conditions, the distribution of zeros of the Husimi function has been studied in realistic systems, showing its relevance in the characterization of quantum states, in particular, at the quantum transition from order to chaos [11,15–17].

Therefore, in this paper we will study the behavior of the Shannon entropy for the series of avoided crossings that characterize the quantum transition from order to chaos [18], analyzing the results through the corresponding distribution of zeros of the Husimi functions. In order to be able to study and compare the Shannon entropy for discrete and continuous probability, calculations have been performed on a quantized map, the kicked Harper map, since quantum maps feature both cases: Position and momentum representations lead to a discrete probability distribution, while coherent state representation leads to a continuous probability density function (the Husimi function) [13]. Additionally, the studied system, i.e., the kicked Harper quantum map, has become a paradigmatic model in the study of classical and quantum chaos [18–30], and hence it is an adequate choice for our purposes.

The organization of the paper is as follows. In Sec. II the kicked Harper model is described (Sec. II A), Shannon entropy expressions used for discrete and continuous cases are indicated (Sec. II B), and explicit expressions used in quantum calculations are shown (Sec. II C). Next, the obtained results are presented and discussed in Sec. III. Finally, the conclusions are summarized in Sec. IV.

II. SYSTEM DESCRIPTION AND CALCULATIONS**A. Quantum kicked Harper map**

The kicked Harper model is described, in terms of normalized dimensionless coordinates, by means of the Hamiltonian function

$$H(p, q, t) = A \cos(2\pi p) + A \cos(2\pi q) \tau \sum_k \delta(t - k\tau), \quad (1)$$

*fj.arranz@upm.es

†rosamaria.benito@upm.es

‡f.borondo@uam.es

which corresponds to the integrable model proposed by Harper [31] for studying the effect of a uniform magnetic field on the conduction band of a metal but subjected to a τ -periodic impulse, and hence giving a nonintegrable Hamiltonian. The classical motion is confined to a toroidal phase space of area 1, since $(p, q) \in [0, 1)$. Notice that the most general expression for the kicked Harper Hamiltonian allows different values for amplitude in momentum and position terms; however, we will restrict ourselves to the symmetric case in Eq. (1). By integrating the equations of motion for successive kicks, the classical kicked Harper map is obtained:

$$p_{k+1} = p_k + \gamma \sin(2\pi q_k), \quad (2a)$$

$$q_{k+1} = q_k - \gamma \sin(2\pi p_{k+1}), \quad (2b)$$

where parameter $\gamma = 2\pi A\tau$ controls the transition from order to chaos as its value increases.

Eventually, the quantization¹ of the kicked Harper map in Eqs. (2) is given by means of the corresponding quantum time evolution unitary operator [19]

$$\widehat{U}(\widehat{P}, \widehat{Q}) = e^{iN\gamma \cos(2\pi\widehat{Q})} e^{iN\gamma \cos(2\pi\widehat{P})}, \quad (3)$$

with $N = (2\pi\hbar)^{-1}$, such that, in order to hold the quantization conditions, $N \in \mathbb{N}$. The operator in Eq. (3) describes the time evolution of a state $|\psi\rangle_k$ for successive kicks:

$$|\psi\rangle_{k+1} = \widehat{U}|\psi\rangle_k. \quad (4)$$

The quantum map is characterized by the N eigenphases ω_n and corresponding eigenstates $|n\rangle$, obtained from the diagonalization of the time evolution operator

$$\widehat{U}|n\rangle = e^{-i\omega_n}|n\rangle, \quad (5)$$

where $n = 1, \dots, N$. Notice that eigenphases ω_n are defined in a 2π -periodic space, such that $\omega_n \in [-\pi, \pi)$.

B. Shannon entropy

The Shannon entropy was defined, in the framework of the theory of information, in the seminal work of Shannon in Refs. [1,2]. For our purposes, the Shannon entropy S_P for a system described by a discrete probability distribution P_k , with $k = 1, \dots, N$, is given by [1]

$$S_P = -\frac{1}{\log N} \sum_{k=1}^N P_k \log P_k, \quad (6)$$

where $(\log N)^{-1}$ is a normalization factor. The definition in Eq. (6) ensures that $0 \leq S_P \leq 1$, such that $S_P = 0$ for a delta distribution $P_k = \delta_{kk'}$, and $S_P = 1$ for a uniform distribution $P_k = 1/N$.

On the other hand, in the case of a system described by a D -dimensional continuous probability density function $\mathcal{P}(\mathbf{x})$, with $\mathbf{x} \in \sigma$, Shannon defined the so-called *differential entropy* [2]

$$S_P = -\int_{\sigma} dx_1 \cdots dx_D \mathcal{P}(\mathbf{x}) \log \mathcal{P}(\mathbf{x}), \quad (7)$$

¹See Refs. [32,33] for a general discussion of the quantization of classical maps.

where the integration extends over the whole domain σ of variables \mathbf{x} . However, the definition in Eq. (7) is not appropriate for our comparative purposes, since, e.g., differential entropy can take negative values. Instead, we have used a discrete distribution obtained from the probability density function as follows. Assuming, as it will be in our case, a two-dimensional probability density function $\mathcal{P}(x, y)$, the domain σ of variables (x, y) is discretized in $M \times M$ squares with side length ℓ , such that, the probability P'_{ij} over the square (i, j) would be approximately $P'_{ij} = \ell^2 \mathcal{P}(x_i, y_j)$. Moreover, in order to ensure that the discretized distribution P'_{ij} is normalized, it must be divided by $\sum_{ij} P'_{ij}$, leading to the discrete distribution

$$P_{ij} = \frac{\mathcal{P}(x_i, y_j)}{\sum_{i,j=1}^M \mathcal{P}(x_i, y_j)}, \quad (8)$$

which depends on the discretization M . Thereby, the Shannon entropy for a system described by a continuous probability density function $\mathcal{P}(x, y)$ is obtained from Eqs. (6) and (8):

$$S_P = \frac{\mathcal{N}^{-1}}{\log M^2} \left[\mathcal{N} \log \mathcal{N} - \sum_{i,j=1}^M \mathcal{P}(x_i, y_j) \log \mathcal{P}(x_i, y_j) \right], \quad (9)$$

where $\mathcal{N} = \sum_{i,j=1}^M \mathcal{P}(x_i, y_j)$ is the normalization factor. Observe that in Eq. (9) the term $\mathcal{N} \log \mathcal{N}$ ensures that $S_P \geq 0$, while the factor \mathcal{N}^{-1} ensures that $S_P \leq 1$.

C. Calculations

In order to diagonalize the time evolution operator in Eq. (3), discrete momentum $\{|p_k\rangle\}_{k=0}^{N-1}$ and discrete position $\{|q_k\rangle\}_{k=0}^{N-1}$ basis sets have been used, where $p_k = q_k = k/N$, with $N = (2\pi\hbar)^{-1}$. In this way, the momentum-dependent part $\widehat{U}_p(\widehat{P})$ and position-dependent part $\widehat{U}_q(\widehat{Q})$ of the time evolution operator $\widehat{U} = \widehat{U}_q \widehat{U}_p$ are projected on their respective basis sets, such that $\widehat{U} = \widehat{I}_q^+ \widehat{U}_q \widehat{I}_q \widehat{I}_p^+ \widehat{U}_p \widehat{I}_p$, where $\widehat{I}_p = \sum_{k=0}^{N-1} |p_k\rangle\langle p_k|$ and $\widehat{I}_q = \sum_{k=0}^{N-1} |q_k\rangle\langle q_k|$ are the corresponding projectors. Thus, given the scalar product between discrete momentum and discrete position vectors

$$\begin{aligned} \langle p_j | q_k \rangle &= \sqrt{2\pi\hbar} e^{-ip_j q_k / \hbar} \\ &= \frac{1}{\sqrt{N}} e^{-i2\pi jk/N}, \end{aligned} \quad (10)$$

matrix elements of the time evolution operator in discrete position representation $\widehat{U} = \sum_{j,k=0}^{N-1} |q_j\rangle\langle q_j| \widehat{U} |q_k\rangle\langle q_k|$ will be

$$\begin{aligned} \langle q_j | \widehat{U} | q_k \rangle &= \langle q_j | \widehat{I}_q^+ \widehat{U}_q \widehat{I}_q \widehat{I}_p^+ \widehat{U}_p \widehat{I}_p | q_k \rangle \\ &= \frac{1}{N} e^{iN\gamma \cos(j2\pi/N)} F_{(k-j)}, \end{aligned} \quad (11)$$

where

$$F_{(k-j)} = \sum_{k'=0}^{N-1} e^{-i2\pi k'(k-j)/N} e^{iN\gamma \cos(k'2\pi/N)} \quad (12)$$

is the discrete Fourier transform of $f_{k'} = e^{iN\gamma \cos(k'2\pi/N)}$. Eventually, the matrix representation in Eq. (11) is diagonalized

by using standard methods [34], leading to the N eigenphases ω_n and corresponding eigenvectors in discrete position representation $\langle q_k|n\rangle$ indicated in Eq. (5). Shannon entropy is calculated assuming $P_k = |\langle q_{k-1}|n\rangle|^2$, with $k = 1, \dots, N$, eigenvectors being previously normalized, and applying the definition in Eq. (6).

On the other hand, the Husimi function, i.e., the probability density function in the coherent state representation, is obtained from the position representation by means of a basis set change, as was shown by Leboeuf and Voros [13]. The (continuous) position representation $\langle q|n\rangle$ of an eigenstate $|n\rangle$ is obtained from its discrete position representation $\langle q_k|n\rangle$ by means of the discrete position projection $\langle q|\hat{I}_q|n\rangle$,

$$\langle q|n\rangle = \sum_{k=0}^{N-1} \langle q|q_k\rangle \langle q_k|n\rangle, \quad (13)$$

where continuous and discrete position basis sets are related by the scalar product

$$\langle q|q_k\rangle = \sum_{\nu=-\infty}^{+\infty} \delta(q - q_k - \nu). \quad (14)$$

Observe that infinity summation in Eq. (14) periodically extends the Dirac delta $\delta(q - q_k)$ in a unit cell on the whole real line supporting the continuous position basis set. Similarly, the coherent state representation $\langle z|n\rangle$ of an eigenstate $|n\rangle$ is obtained from the position representation $\langle q|n\rangle$ through the position projection

$$\langle z|n\rangle = \int dq \langle z|q\rangle \langle q|n\rangle, \quad (15)$$

where coherent states and position basis sets are related by the scalar product

$$\langle z|q\rangle = (2N)^{1/4} e^{-\pi N(z^2 + q^2)} e^{\pi N 2\sqrt{2}zq}, \quad (16)$$

where $z = (\bar{q} - i\bar{p})/\sqrt{2}$ a complex number characterizing the coherent state, such that $\bar{q} = \langle z|\hat{Q}|z\rangle$ and $\bar{p} = \langle z|\hat{P}|z\rangle$ are the expectation values of position and momentum operators, respectively. Notice that coherent state in Eq. (16) is not normalized, since $\langle z|z\rangle = \exp(2\pi N|z|^2)$. From Eqs. (13)–(16) the following explicit expression for the coherent state representation of an eigenstate in discrete position representation $\langle q_k|n\rangle$ is achieved:

$$\begin{aligned} \langle z|n\rangle &= (2N)^{1/4} \sum_{k=0}^{N-1} \vartheta_3((-i\pi N(\sqrt{2}z - k/N) | iN)) \\ &\times e^{-\pi N[z^2 + (k/N)^2]} e^{\pi 2\sqrt{2}zk} \langle q_k|n\rangle, \end{aligned} \quad (17)$$

where

$$\vartheta_3(u | \tau) = \sum_{\nu=-\infty}^{+\infty} e^{i2u\nu} e^{i\pi \tau \nu^2} \quad (18)$$

is the third Jacobi theta function [35]. Eventually the Husimi function $\mathcal{H}(z)$ is obtained by normalizing the coherent state representation $\mathcal{H}(z) = |\langle z|n\rangle|^2 / \exp(2\pi N|z|^2)$, and Shannon entropy is calculated assuming $\mathcal{P}(x, y) = \mathcal{H}(\bar{q}, \bar{p})$, with $z = (\bar{q} - i\bar{p})/\sqrt{2}$, and applying the discretization indicated in Eqs. (8) and (9).

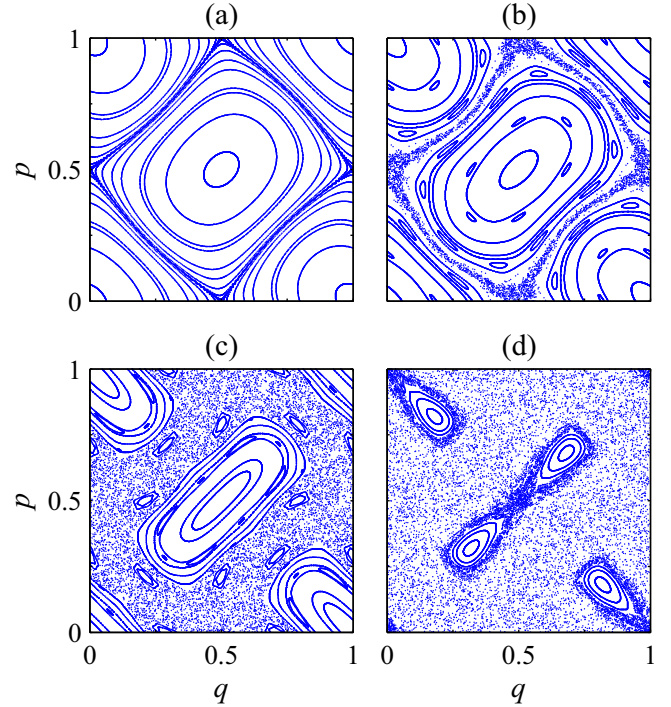


FIG. 1. Classical kicked Harper map given, with random initial conditions, obtained for increasing control parameter values $\gamma = 0.1$ (a), $\gamma = 0.2$ (b), $\gamma = 0.3$ (c), and $\gamma = 0.4$ (d).

III. RESULTS AND DISCUSSION

In order to have a clear picture of the system, such that quantum eigenstates can be identified with the corresponding quantized classical structures, the classical dynamics of the kicked Harper map in Eq. (2), with random initial conditions, is represented in Fig. 1 for increasing values of the control parameter γ . Observe that, indeed, as parameter γ increases, regular tori are progressively destroyed while simultaneously the chaotic sea grows. For $\gamma \gtrsim 0.63$ the dynamics is dominated by chaotic trajectories [19]. Note also the toroidal symmetry of the phase space, as was claimed in Sec. II A. Moreover, there exists additional symmetry in phase space, namely, each point (q, p) can be rotated $\pm\pi/2$, translated $\pm 1/2$, and folded into the unit cell $[0, 1)$, such that the corresponding symmetric point is obtained. In particular, we can observe in Fig. 1 this symmetry relation between both main torus families: the *central* torus family, formed by tori located around the central fixed point $(q_c, p_c) = (1/2, 1/2)$, and the *corner* torus family, formed by tori located around the corner fixed point $(q_v, p_v) = (0, 0) = (0, 1) = (1, 0) = (1, 1)$ (note that, due to the toroidal symmetry, the four vertices correspond to the same point in the phase space).

Moreover, the spectrum obtained from the eigenvalue equation (5) by taking $N = 30$ in Eq. (3) is depicted in Fig. 2 as a function of parameter γ . Eigenphases with positive slope $(d\omega_n/d\gamma) > 0$ correspond to states quantized on the central torus family in Fig. 1, while eigenphases with negative slope $(d\omega_n/d\gamma) < 0$ correspond to states quantized on the corner torus family. In each case, the maximum absolute slope corresponds to the ground state, and the minimum absolute

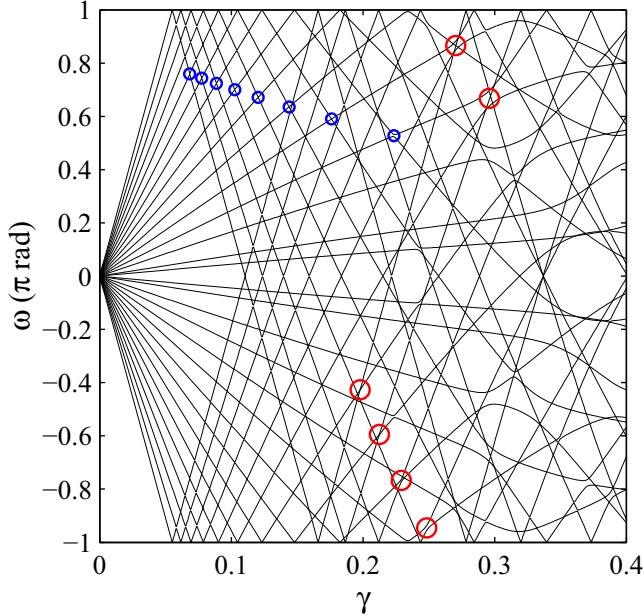


FIG. 2. Eigenphase spectrum ω_n versus parameter γ for $N = 30$. The two series of avoided crossings studied are marked with open circles. Blue (smaller) circles correspond to hetero-resonances between states quantized on different torus families, and red (bigger) circles correspond to homo-resonances between states quantized on the same torus family.

slope corresponds to the maximum excited state. Observe the cylindrical symmetry of the eigenphase spectrum, such that, when an eigenphase with negative slope reaches $\omega = -\pi$ rad, it continues from value $\omega = \pi$ rad, and conversely for an eigenphase with positive slope. This behavior results in the occurrence of (avoided) crossings between states quantized on both the central torus and corner torus families. Thus, the avoided crossings in this regular region of the spectrum can be classified into two classes: The *hetero-resonances*, that correspond to avoided crossings between states quantized on different torus families, and the *homo-resonances*, that correspond to avoided crossings between states quantized on the same torus family. Notice that, as parameter γ increases, the avoided crossings gap also increases, such that for $\gamma \gtrsim 0.3$ the overlap of avoided crossings breaks down the linear behavior of the spectrum, leading to the onset of quantum chaos. We should point out that this threshold corresponds to the chosen value $N = 30$. Indeed, the onset of quantum chaos depends on the Planck constant [hence on $N = (2\pi\hbar)^{-1}$], such that, as \hbar decreases (hence N increases), the threshold value of γ increases.

We focus on two series of avoided crossings that characterize the transition from order to chaos in this system [18]. The first series corresponds to hetero-resonances between states quantized on the central torus family, with quantum number $n_c = 4 + k$, and states quantized on the corner torus family, with quantum number $n_v = k$, where $k = 0, \dots, 7$, resulting in the order of resonance $\rho = |n_c - n_v| = 4$. The second series corresponds to homo-resonances between states quantized on central torus family, with quantum numbers $n_c = 6 + k$ and $n'_c = k$, where $k = 0, \dots, 5$, resulting in the

order of resonance $\rho = |n_c - n'_c| = 6$. Both series have been marked in Fig. 2 with blue (smaller) and red (bigger) circles, respectively. Observe that the ninth avoided crossing in the 4-resonance series and the seventh avoided crossing in the 6-resonance series, both not marked in Fig. 2, overlap at $(\gamma, \omega) \approx (0.3, 0.4\pi$ rad) establishing the onset of quantum chaos. In this case, the state quantized on the central torus family with quantum number $n_c = 12$, which is shared by both avoided crossings, interacts with the state quantized on the corner torus family with quantum number $n_v = 8$, leading to a broad avoided crossing, such that before the completion of the avoided crossing, it again interacts, in a broader avoided crossing, with the state quantized on the central torus family with quantum number $n'_c = 6$, resulting in the overlapping of both avoided crossings. After these overlapped avoided crossings, no more avoided crossings are in both series, since, due to the progressive destruction of tori as parameter γ increases, the corresponding quantization is not supported, and the system enters into the quantum chaotic region. Due to this overlap, both avoided crossings have been excluded from the following Shannon entropy calculations, since states from different series are mixing, and consequently the related Shannon entropy will also be mixing, and then it will not be adequate to study separately the behavior in both hetero- and homo-resonances series.

Shannon entropy calculations for the hetero-resonance series, along with magnifications of the corresponding avoided crossing, are represented in Fig. 3, where spectrum coordinates (γ, ω) have been shifted to the center of each avoided crossing. The parameters determining each avoided crossing are listed in Table I. Observe that, as indicated by the different orders of magnitude in the values of $\tilde{\gamma}$ and $\tilde{\omega}$ (see $\tilde{\omega}_b$ values) represented in Fig. 6 below, avoided crossings evolve from very narrow to broader avoided crossings in the series. In this regard, note that in Fig. 1 only the gap of the last avoided crossing is perceptible. Consequently, the appropriate number of significant figures of the values given in Table I decreases in the series.

The results of Shannon entropy for the continuous case (Husimi function) were obtained by taking the discretization $M = 100$ in Eqs. (8) and (9). Observe that, as the center γ_0 of the corresponding avoided crossing increases (first crossing, second crossing, etc.), the behavior of the Shannon entropy for Husimi probability density evolves monotonously, as should be expected. Indeed, each avoided crossing implies the exchange of character between both involved states, such that the corresponding Shannon entropy is also exchanged. Since Shannon entropy is a measure of the delocalization of the wave function, the progressive increase of its value in the series is due to the progressive increase of the involved quantum numbers (see Table I), and hence the increase of the delocalization of the corresponding wave functions. Additionally, we can observe that, around the center of the avoided crossings, Shannon entropy reaches a maximum for both involved states. Notice that, in the hetero-resonance series, avoided crossings mix states quantized on the two different torus families, such that resulting mixed states are delocalized over both torus families, hence giving a higher value of Shannon entropy. These assertions can be verified in Figs. 4 and 5, where the Husimi function of the states involved in the first and eighth

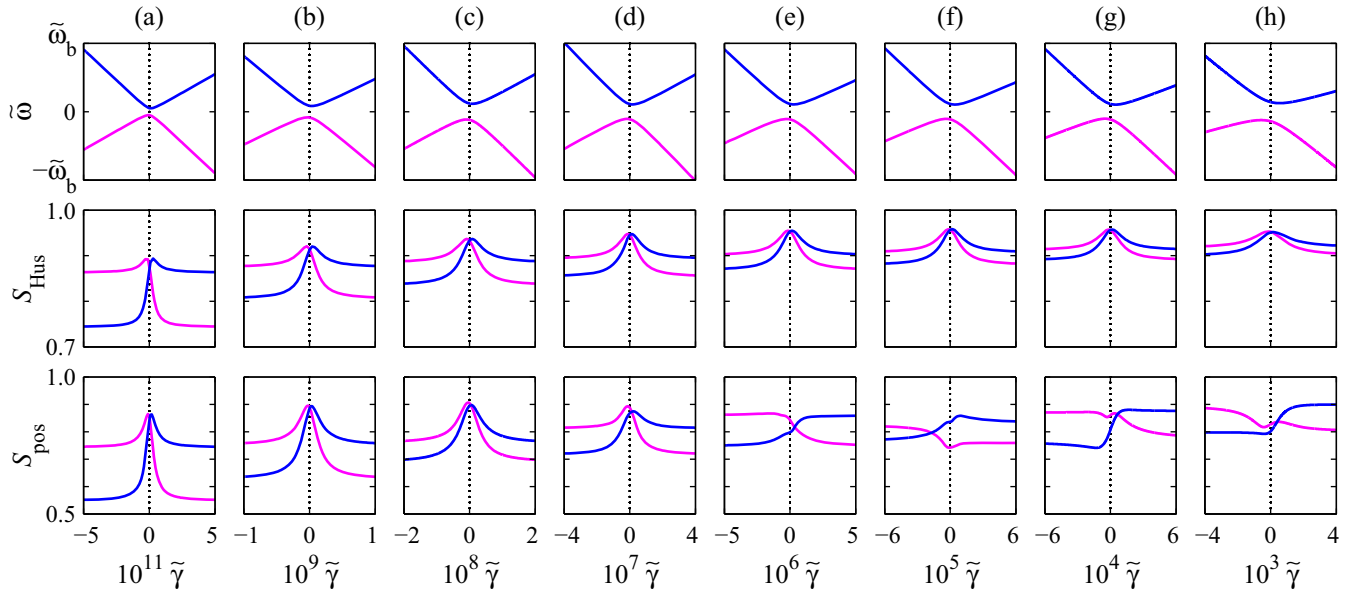


FIG. 3. Magnification of the avoided crossings (top panels) in the hetero-resonance series, along with the corresponding Shannon entropy of the involved states for Husimi probability density (middle panels) and for position probability (bottom panels). Columns (a)–(h) correspond to the first through eighth avoided crossing, respectively, in the series. Blue (dark gray) and magenta (light gray) lines correspond to upper and lower states, respectively, in the avoided crossings. Coordinates $\tilde{\gamma} = \gamma - \gamma_0$ and $\tilde{\omega} = \omega - \omega_0$ shifted to the center (γ_0, ω_0) of each avoided crossing have been used. Parameter $\tilde{\omega}_b$ defines the different boundaries for the $\tilde{\omega}$ coordinate used in each magnification. All parameters determining each avoided crossing are listed in Table I.

avoided crossing in the series, respectively, are depicted. Thus, in the first avoided crossing, the highly localized state $n_v = 0$ (lower Shannon entropy) and the less localized state $n_c = 4$ (higher Shannon entropy) interact, giving states delocalized over the two torus families (highest Shannon entropy in the avoided crossing). However, in the last avoided crossing, both interacting states, $n_v = 7$ and $n_c = 11$, have a similar low degree of localization (hence a nearby high Shannon entropy), resulting in two states highly delocalized over the separatrix region between the two torus families.

On the other hand, as can be observed in Fig. 3, the evolution of the behavior of the Shannon entropy for position probability is somewhat different. In the first three avoided crossings, the Shannon entropy for discrete and continuous probability evolves qualitatively in a similar fashion, albeit quantitatively the differences between values before, during,

and after the avoided crossing are conspicuous. In the fourth avoided crossing, the symmetry existing between both upper and lower states curves is lost, the maximum reached by lower state curve being slightly higher than that reached by upper state curve. Finally, in the last four avoided crossings, the behavior of Shannon entropy curves for discrete probability is completely different from the corresponding to continuous probability, some curves having a minimum rather than a maximum, and even both a minimum and a maximum, in the vicinity of the avoided crossing point. This different behavior of Shannon entropy curves is a consequence of the different behavior of position and Husimi probability distributions at the avoided crossings as involved quantum numbers increase. For low quantum numbers, the position probability distributions before and after the avoided crossing are almost completely exchanged, and at the avoided crossing point they are practically the same, as can be observed for the first avoided crossing in Fig. 4. However, for higher quantum numbers, the position probability distributions are not completely exchanged, such that the distribution of the upper state (lower state) before the avoided crossing and the distribution of the lower state (upper state) after the avoided crossing are similar but different. In the same way, at the avoided crossing point both distributions are also similar but clearly different. Both assertions can be observed in Fig. 5 for the last avoided crossing in the series. Later we will explain this different behavior in terms of the distribution of zeros of the Husimi function, but before that, we will discuss the results for the homo-resonance series.

Shannon entropy calculations for the homo-resonance series, along with magnifications of the corresponding avoided crossing, are represented in Fig. 6, where spectrum coordinates (γ, ω) , as in the hetero-resonance series case,

TABLE I. Parameters determining each avoided crossing (AC) in the hetero-resonance series: involved quantum numbers (n_c, n_v) , center of the avoided crossing (γ_0, ω_0) , and boundaries $\tilde{\omega}_b$ used in magnifications depicted in Fig. 3.

AC	n_c	n_v	γ_0	ω_0 (π rad)	$\tilde{\omega}_b$ (π rad)
1st	4	0	0.068451065683	0.759813181437	0.000000001
2nd	5	1	0.07755589088	0.74325946978	0.00000002
3rd	6	2	0.0887057021	0.7236916217	0.0000003
4th	7	3	0.10262581	0.70020610	0.000005
5th	8	4	0.1204260	0.6715196	0.00006
6th	9	5	0.14391	0.63564	0.0006
7th	10	6	0.17614	0.59014	0.005
8th	11	7	0.2235	0.5277	0.03

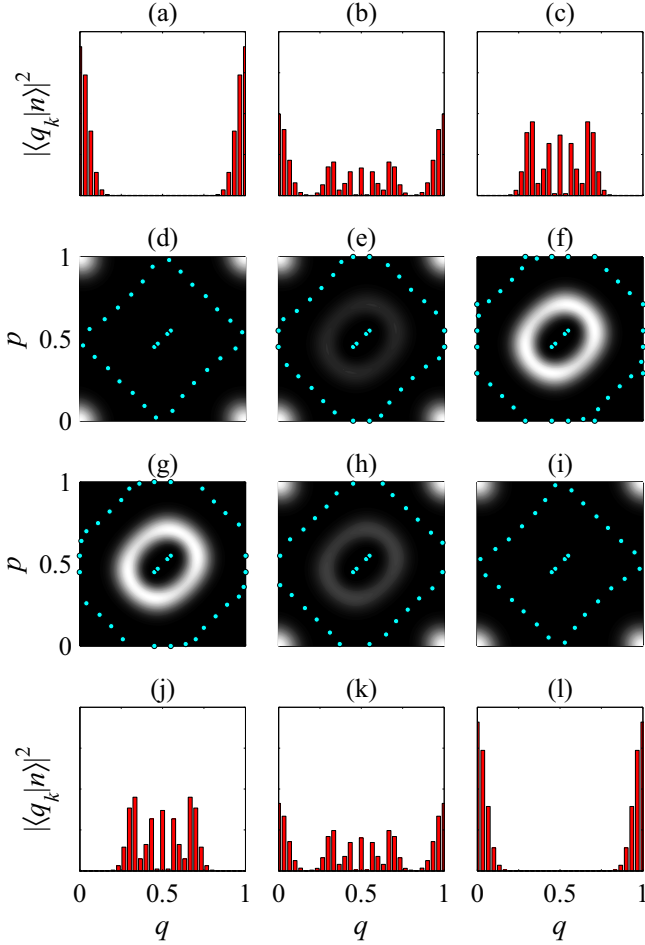


FIG. 4. Upper state [upper panels: (a)–(f)] and lower state [lower panels: (g)–(l)] involved in the first avoided crossing in the hetero-resonance series, represented before [left panels: (a), (d), (g), and (j)], during [central panels: (b), (e), (h), and (k)], and after [right panels: (c), (f), (i), and (l)] the avoided crossing. Histograms [(a)–(c) and (j)–(l)] represent the probability in position representation, and grayscale depictions [(d)–(i)] represent the probability density in the coherent state representation (Husimi function). Zeros of the Husimi function have been marked with cyan (grayish-white) dots.

have been shifted to the center of the avoided crossing. Parameters determining each avoided crossing are listed in Table II. Observe that, similarly to the hetero-resonance series case, avoided crossings evolve from narrow to broader avoided crossings in the series. However, in this case the differences between the first and the last avoided crossings are much smaller, such that the orders of magnitude in the values of $\tilde{\gamma}$ and $\tilde{\omega}$ represented in Fig. 6 are similar. Thereby, the appropriate number of significant figures of the values given in Table II is also similar. Accordingly, note that in Fig. 1 the increase of the avoided crossing gap in the series is clearly perceptible in this case.

The results of Shannon entropy for the continuous case (Husimi function) were obtained, as in the hetero-resonance series case, by taking the discretization $M = 100$ in Eqs. (8) and (9). Note that, similarly to in the hetero-resonance series, Shannon entropy for Husimi probability density evolves monotonously, increasing its value as quantum numbers

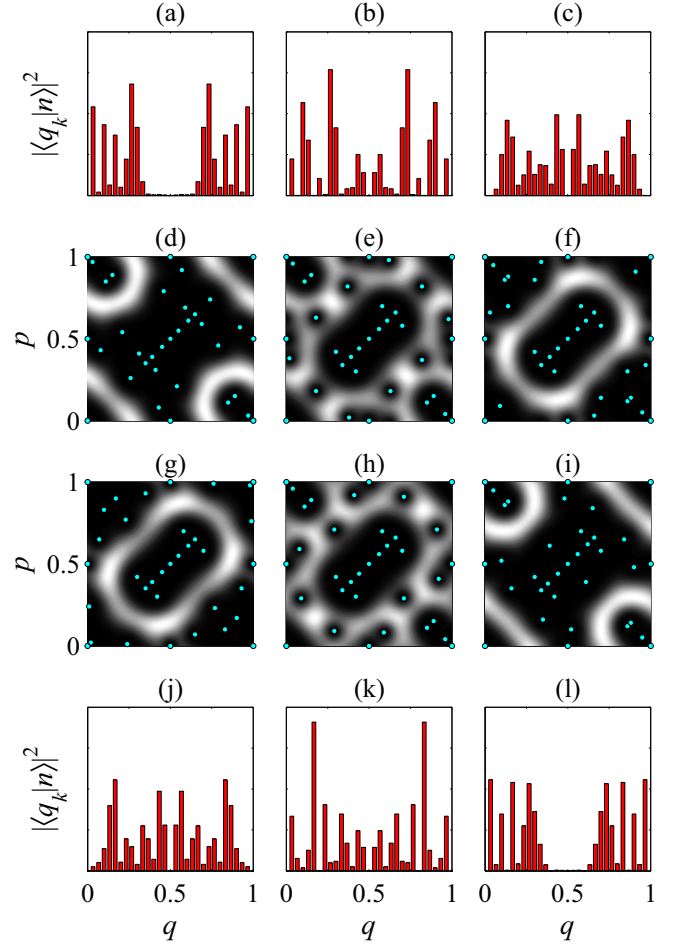


FIG. 5. Same as described in the caption of Fig. 4 for the eighth avoided crossing in the hetero-resonance series.

increase, with the involved states exchanging their character and then their corresponding Shannon entropy. However, in this case the maximum of Shannon entropy around the center of the avoided crossing is nearly negligible, the shape of the curves being quasisigmoid. As was shown for the first time in molecular systems [11,16], and later in the kicked Harper map [18], the transition order-to-chaos is characterized by a series of avoided crossings, related to complementary stable and unstable periodic orbits, where some zeros of the Husimi function move to the corresponding elliptic and hyperbolic points, and conversely probability density accumulates around hyperbolic (*scarred* state) and elliptic points in each case. As a consequence, in particular as quantum numbers increase, the localization (and then Shannon entropy) for the more excited state and for resulting states is similar. These observations can be verified in Figs. 7 and 8, where the Husimi function of the states involved in the first and sixth avoided crossing in the series, respectively, is depicted. Observe that, in the first avoided crossing, the highly localized state $n'_c = 0$ (lower Shannon entropy) and the less localized state $n_c = 6$ (higher Shannon entropy) interact, giving states with six zeros at elliptic and hyperbolic points (see the chain of six islands in Fig. 1 for $\gamma = 0.2$ and $\gamma = 0.3$), and with part of the probability density accumulated around hyperbolic and

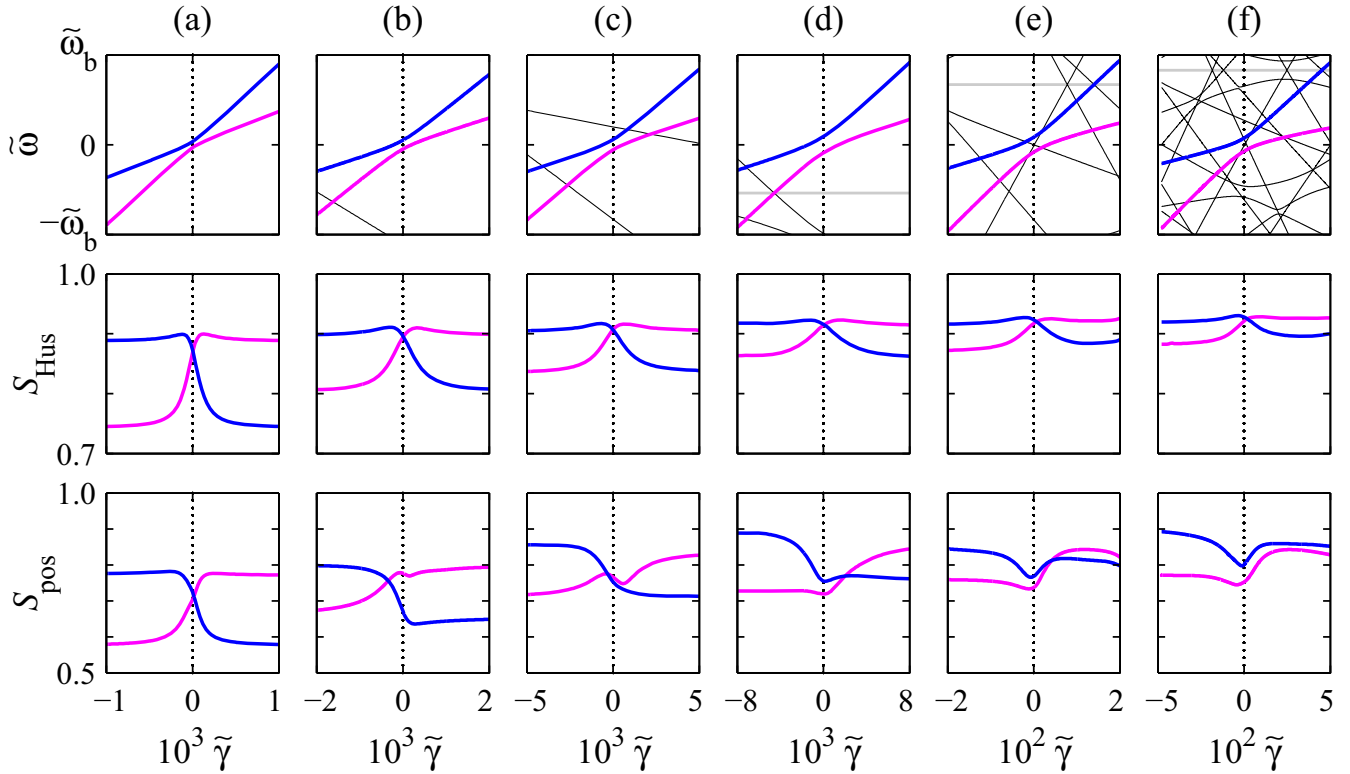


FIG. 6. Same as described in the caption of Fig. 3 for the homo-resonance series. Columns (a)–(f) correspond to the first through sixth avoided crossing, respectively, in the series. Horizontal gray line in the fourth, fifth, and sixth avoided crossings corresponds to symmetry line $\omega = \pm\pi$ rad. All parameters determining each avoided crossing are listed in Table II.

elliptic points, albeit in this case maximum probability density is at the center of the torus family. However, as quantum numbers increase, the maximum probability density tends to be localized on the hyperbolic and elliptic points, as is the case for the last avoided crossing, where states $n'_c = 5$ and $n_c = 11$ are mixed, giving two states clearly localized on the corresponding unstable and stable 6-resonance periodic orbits.

On the other hand, as was the case for the hetero-resonance series, the evolution of Shannon entropy in the homo-resonance series for position probability is different from that for Husimi function. In this case, as can be observed in Fig. 6, the behavior of Shannon entropy for discrete probability is similar to, albeit quantitatively lower than, that for continuous

probability only in the first avoided crossing. In the rest of the avoided crossings, the evolution of Shannon entropy curves for both discrete and continuous cases are completely different, and observations similar to those for the hetero-resonance series can be made, in particular, the differentiation of both cases as quantum numbers increase. In this regard, it is interesting to point out that both the hetero-resonance series and the homo-resonance series support similar behavior of Shannon entropy curves for discrete and continuous cases when the higher quantum number involved is less than or equal to six, i.e., when the maximum number of zeros of the Husimi function inside the corresponding torus is six (the first, second, and third avoided crossings in the hetero-resonance series, and only the first avoided crossing in the homo-resonance series).

In order to illustrate the causes of the different behavior of position and Husimi probabilities in the avoided crossings, as well as of the corresponding Shannon entropy, we will focus on the second avoided crossing in the homo-resonance series, where the Shannon entropy difference between both involved states at the center of the avoided crossing is the highest in the series for position probability, while it is virtually null (i.e., the same Shannon entropy) for Husimi probability density (see Fig. 6). The corresponding position and Husimi probabilities at the avoided crossing point are depicted in Fig. 9. Note that the position coordinate in continuous Husimi probability density has been discretized in 30 strips, corresponding to the 30 bins of the discrete position probability [due to the choice $N = 30$ in Eq. (3) for our calculations]. Despite the fact that,

TABLE II. Parameters determining each avoided crossing (AC) in the homo-resonance series: Involved quantum numbers (n_c, n'_c), center of the avoided crossing (γ_0, ω_0), and boundaries $\tilde{\omega}_b$ used in magnifications depicted in Fig. 6.

AC	n_c	n'_c	γ_0	ω_0 (π rad)	$\tilde{\omega}_b$ (π rad)
1st	6	0	0.19782	-0.42736	0.02
2nd	7	1	0.21248	-0.59463	0.04
3rd	8	2	0.2292	-0.7672	0.08
4th	9	3	0.2484	-0.9461	0.1
5th	10	4	0.2705	0.8660	0.2
6th	11	5	0.2960	0.6678	0.4

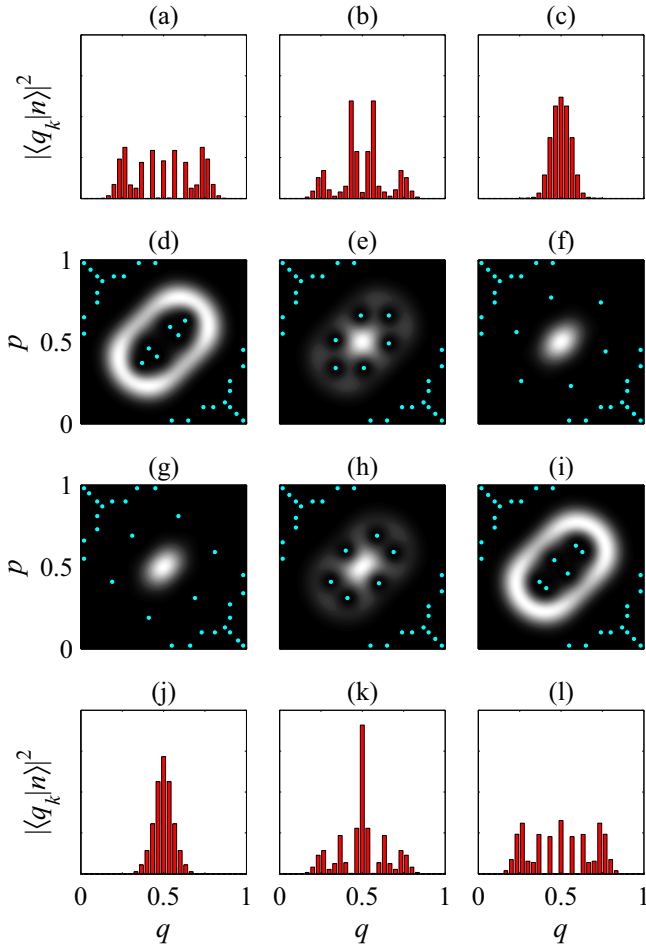


FIG. 7. Same as described in the caption of Fig. 4 for the first avoided crossing in the homo-resonance series.

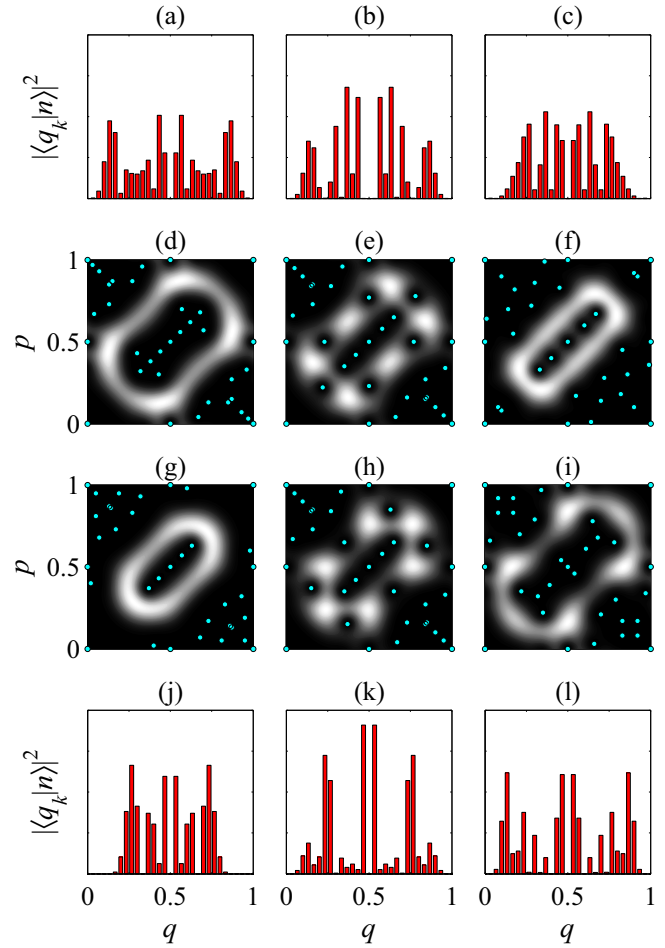


FIG. 8. Same as described in the caption of Fig. 4 for the sixth avoided crossing in the homo-resonance series.

strictly speaking, position probability cannot be obtained from the projection of the position coordinate in Husimi probability density, it can be obtained *approximately*. Indeed, as is well known [36], position and momentum probabilities can be obtained from the projection of position or momentum coordinates in Wigner quasiprobability density, and the Husimi function can be obtained from a Gaussian smoothing of the Wigner function, such that we can consider the projection of the position coordinate in the Husimi function as a qualitative approximation to the position probability. With this assumption in mind, the following qualitative analysis is made.

We can observe in Fig. 9 that the distribution of zeros of the Husimi function for both states is the same, except for the six zeros corresponding to the elliptic (upper state) and hyperbolic (lower state) points of the 6-resonance previously pointed out. Thus, for these six differences, where the upper state has a zero, the lower state accumulates probability density, and conversely, where the upper state accumulates probability density, the lower state has a zero. Therefore, the Husimi function of both the upper and lower states has almost the same localization degree, and hence the corresponding Shannon entropy has almost the same value. However, when projected on the position coordinate, both states give different results. Indeed, maximum probability in position

representation for the upper state corresponds to the symmetric positions $k = 12$ and $k = 18$, the corresponding strips in the Husimi function containing the maximum probability densities, regions where probability density accumulates, and only one zero (each strip) in the region where probability density is negligible. Then, when projected on the position coordinate, they give the highest values. On the other hand, the symmetric positions $k = 12$ and $k = 18$ for the lower state correspond to local minima in position probability, since in this case the corresponding strips in the Husimi function contain two additional zeros (those located on hyperbolic points), such that, when projected on the position coordinate, they give small probability values. This qualitative analysis can be made for all discrete positions in each pair of states involved in the series of avoided crossings (considering also the adjacent strips in each case in order to take into account the Gaussian smoothing noted above), such that the different probability distributions for position and Husimi cases can be understood, and hence the corresponding Shannon entropy differences can be also understood. In summary, the distribution of zeros of the Husimi function would explain the differences found in the Shannon entropy of the states involved in an avoided crossing for discrete position representation and for continuous coherent states representation.

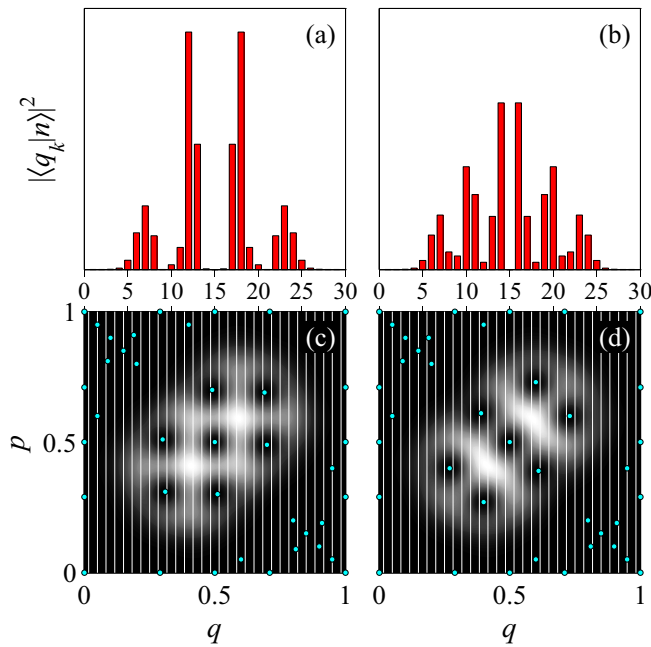


FIG. 9. Upper state [left panels: (a) and (c)] and lower state [right panels: (b) and (d)] involved in the second avoided crossing in the homo-resonance series, represented at the center of the avoided crossing. Histograms [(a) and (b)] represent the probability in position representation, and grayscale depictions [(c) and (d)] represent the probability density in the coherent state representation (Husimi function). Zeros of the Husimi function have been marked with cyan (grayish-white) dots. Vertical lines superimposed on the continuous Husimi function correspond to the histogram bin width of the discrete position representation. The index $k = 0, 1, \dots, 30$ labeling the discrete positions q_k has been included. Note that $k = 0$ and $k = 30$ label the same position $q_0 = 0$.

IV. SUMMARY AND CONCLUSIONS

We have studied the behavior of Shannon entropy in the series of avoided crossings that characterize the quantum

transition from order to chaos in the quantized kicked Harper map. Since the states of a quantized map allow both discrete and continuous representation, we have calculated and compared Shannon entropy for discrete (position representation) and continuous (coherent states representation) cases, obtaining different results.

Up to a certain threshold in the quantum excitation [$n_c = 6$ in our case for $N = (2\pi\hbar)^{-1} = 30$], the behavior of Shannon entropy for discrete and continuous cases has qualitatively the same monotonous evolution in the series. However, when this threshold is exceeded, the qualitative behavior of Shannon entropy for the discrete position representation detaches from the monotonous evolution of the continuous case, indicating the closeness of the frontier between order and chaos in the system.

This different behavior is explained in terms of the total (continuous case) or partial (discrete case) exchange of character of the involved states as the system approaches the chaotic region, which in turn is understood in terms of the distribution of zeros of the Husimi function (probability density in the coherent states representation).

Last, as a corollary, it is worth noting that Shannon entropy is not a property of the quantum state, but it is a property of the quantum state representation used (it measures the degree of probability delocalization for the corresponding probability function). Indeed, a property of a given state does not depend on the representation used (e.g., position expectation value of a state is the same in all representations), while Shannon entropy depends on the representation, as has been shown in our results for both position and coherent state representations.

ACKNOWLEDGMENTS

This research was supported by the Ministry of Economy and Competitiveness of Spain under Grant No. MTM2015-63914-P and by ICMAT Severo Ochoa under Contract SEV-2015-0554.

- [1] C. E. Shannon, A mathematical theory of communication, *Bell. Syst. Tech. J.* **27**, 379 (1948).
- [2] C. E. Shannon, A mathematical theory of communication, *Bell. Syst. Tech. J.* **27**, 623 (1948).
- [3] L. E. Reichl, *The Transition to Chaos—Conservative Classical Systems and Quantum Manifestations* (Springer-Verlag, New York, 2004).
- [4] R. González-Férez and J. S. Dehesa, Diamagnetic informational exchange in hydrogenic avoided crossings, *Chem. Phys. Lett.* **373**, 615 (2003).
- [5] R. González-Férez and J. S. Dehesa, Shannon Entropy as an Indicator of Atomic Avoided Crossings in Strong Parallel Magnetic and Electric Fields, *Phys. Rev. Lett.* **91**, 113001 (2003).
- [6] W. Jian-Jie, Shannon entropy as a measurement of the information in a multiconfiguration Dirac-Fock wavefunction, *Chin. Phys. Lett.* **32**, 023102 (2015).
- [7] Y. L. He, Y. Chen, J. N. Han, Z. B. Zhu, G. X. Xiang, H. D. Liu, B. H. Ma, and D. C. He, Shannon entropy as an indicator of atomic avoided crossings for Rydberg potassium atoms interacting with a static electric field, *Eur. Phys. J. D* **69**, 283 (2015).
- [8] E. J. Torres-Herrera and L. F. Santos, Dynamical manifestations of quantum chaos: Correlation hole and bulge, *Phil. Trans. R. Soc. A* **375**, 20160434 (2017).
- [9] K.-W. Park, S. Moon, Y. Shin, J. Kim, K. Jeong, and K. An, Shannon entropy and avoided crossings in closed and open quantum billiards, *Phys. Rev. E* **97**, 062205 (2018).
- [10] F. J. Arranz, F. Borondo, and R. M. Benito, Avoided crossings, scars, and transition to chaos, *J. Chem. Phys.* **107**, 2395 (1997).
- [11] F. J. Arranz, F. Borondo, and R. M. Benito, Scar Formation at the Edge of the Chaotic Region, *Phys. Rev. Lett.* **80**, 944 (1998).
- [12] F. J. Arranz, L. Seidel, C. G. Giralda, R. M. Benito, and F. Borondo, Scars at the edge of the transition from order to chaos in the isomerizing molecular systems LiNC-LiCN and HCN-HNC, and HO₂, *Phys. Rev. E* **82**, 026201 (2010).

- [13] P. Leboeuf and A. Voros, Chaos-revealing multiplicative representation of quantum eigenstates, *J. Phys. A* **23**, 1765 (1990).
- [14] S. Nonnenmacher and A. Voros, Chaotic eigenfunctions in phase space, *J. Stat. Phys.* **92**, 431 (1998).
- [15] M. B. Cibils, Y. Cuche, P. Leboeuf, and W. F. Wreszinski, Zeros of the Husimi functions of the spin-boson model, *Phys. Rev. A* **46**, 4560 (1992).
- [16] F. J. Arranz, F. Borondo, and R. M. Benito, Distribution of zeros of the Husimi function in a realistic Hamiltonian molecular system, *Phys. Rev. E* **54**, 2458 (1996).
- [17] F. J. Arranz, L. Seidel, C. G. Giralda, R. M. Benito, and F. Borondo, Onset of quantum chaos in molecular systems and the zeros of the Husimi function, *Phys. Rev. E* **87**, 062901 (2013).
- [18] D. A. Wisniacki, M. Saraceno, F. J. Arranz, R. M. Benito, and F. Borondo, Poincaré-Birkhoff theorem in quantum mechanics, *Phys. Rev. E* **84**, 026206 (2011).
- [19] P. Leboeuf, J. Kurchan, M. Feingold, and D. P. Arovos, Phase-Space Localization: Topological Aspects of Quantum Chaos, *Phys. Rev. Lett.* **65**, 3076 (1990).
- [20] R. Artuso, G. Casati, and D. Shepelyansky, Fractal Spectrum and Anomalous Diffusion in the Kicked Harper Model, *Phys. Rev. Lett.* **68**, 3826 (1992).
- [21] R. Ketzmerick, G. Petschel, and T. Geisel, Slow Decay of Temporal Correlations in Quantum Systems with Cantor Spectra, *Phys. Rev. Lett.* **69**, 695 (1992).
- [22] R. Artuso, F. Borgonovi, I. Guarneri, L. Rebuzzini, and G. Casati, Phase Diagram in the Kicked Harper Model, *Phys. Rev. Lett.* **69**, 3302 (1992).
- [23] R. Roncaglia, L. Bonci, F. M. Izrailev, B. J. West, and P. Grigolini, Tunneling Versus Chaos in the Kicked Harper Model, *Phys. Rev. Lett.* **73**, 802 (1994).
- [24] P. Leboeuf and A. Mouchet, Tunneling and the Band Structure of Chaotic Systems, *Phys. Rev. Lett.* **73**, 1360 (1994).
- [25] I. Dana, Quantum Suppression of Diffusion on Stochastic Webs, *Phys. Rev. Lett.* **73**, 1609 (1994).
- [26] R. Ketzmerick, K. Kruse, and T. Geisel, Avoided Band Crossings: Tuning Metal-Insulator Transitions in Chaotic Systems, *Phys. Rev. Lett.* **80**, 137 (1998).
- [27] I. I. Satija and B. Sundaram, Quantized Orbits and Resonant Transport, *Phys. Rev. Lett.* **84**, 4581 (2000).
- [28] C. Eltschka and P. Schlagheck, Resonance- and Chaos-Assisted Tunneling in Mixed Regular-Chaotic Systems, *Phys. Rev. Lett.* **94**, 014101 (2005).
- [29] J. Gong and P. Brumer, Generic Quantum Ratchet Accelerator with Full Classical Chaos, *Phys. Rev. Lett.* **97**, 240602 (2006).
- [30] J. Wang, I. Guarneri, G. Casati, and J. Gong, Long-Lasting Exponential Spreading in Periodically Driven Quantum Systems, *Phys. Rev. Lett.* **107**, 234104 (2011).
- [31] P. G. Harper, Single band motion of conduction electrons in a uniform magnetic field, *Proc. Phys. Soc. A* **68**, 874 (1955).
- [32] M. V. Berry, N. L. Balazs, M. Tabor, and A. Voros, Quantum maps, *Ann. Phys.* **122**, 26 (1979).
- [33] I. Dana, General quantization of canonical maps on a two-torus, *J. Phys. A* **35**, 3447 (2002).
- [34] E. Anderson, Z. Bai, C. Bischof, S. Blackford, J. Demmel, J. Dongarra, J. Du Croz, A. Greenbaum, S. Hammarling, A. McKenney, and D. Sorensen, *LAPACK Users' Guide* (SIAM, Philadelphia, 1999).
- [35] E. W. Weisstein, *Encyclopedia of Mathematics* (CRC Press–Chapman & Hall, Boca Raton, FL, 2009).
- [36] H.-W. Lee, Theory and application of the quantum phase-space distribution functions, *Phys. Rep.* **259**, 147 (1995).